energies

MDPI

Article

Implementation of Optimal Two-Stage Scheduling of Energy Storage System Based on Big-Data-Driven Forecasting—An Actual Case Study in a Campus Microgrid

Byeong-Cheol Jeong, Dong-Hwan Shin, Jae-Beom Im, Jae-Young Park and Young-Jin Kim *

Department of Electrical Engineering, Pohang University of Science and Technology (POSTECH), Pohang, Gyungbuk 37673, Korea; jeongbc8874@postech.ac.kr (B.-C.J.); sdhwan05@postech.ac.kr (D.-H.S.); jaebeom@postech.ac.kr (J.-B.I.); luckypark@postech.ac.kr (J.-Y.P.)

* Correspondence: powersys@postech.ac.kr; Tel.: +82-54-279-2368

Received: 15 February 2019; Accepted: 19 March 2019; Published: 22 March 2019

Abstract: Optimal operation scheduling of energy storage systems (ESSs) has been considered as an effective way to cope with uncertainties arising in modern grid operation such as the inherent intermittency of the renewable energy sources (RESs) and load variations. This paper proposes a scheduling algorithm where ESS power inputs are optimally determined to minimize the microgrid (MG) operation cost. The proposed algorithm consists of two stages. In the first stage, hourly schedules during a day are optimized one day in advance with the objective of minimizing the operating cost. In the second stage, the optimal schedule obtained from the first stage is repeatedly updated every 5 min during the day of operation to compensate for the uncertainties in load demand and RES output power. The ESS model is developed considering operating efficiencies and then incorporated in mixed integer linear programming (MILP). Penalty functions are also considered to acquire feasible optimal solutions even under large forecasting errors in RES generation and load variation. The proposed algorithm is verified in a campus MG, implemented using ESSs and photovoltaic (PV) arrays. The field test results are obtained using open-source software and then compared with those acquired using commercial software.

Keywords: energy storage system (ESS); implementation; Internet of Things (IoT); microgrid (MG); microgrid energy management system (MEMS); mixed integer linear programming (MILP); open-source; optimal scheduling; two-stage

1. Introduction

The concept of microgrids (MGs) and corresponding applications have drawn considerable attention from researchers over the last decades, given that it is now possible to reliably and efficiently integrate distributed energy resources (DERs) into today's power systems [1,2]. They can integrate distributed renewable energy generation and storage capacity to meet the electrical needs of customers. They greatly enhance local power supply reliability [3]. However, many challenging issues are associated with MGs operation, the most common of which is the reliable integration of renewable energy sources (RESs), such as photovoltaic (PV) and wind turbine (WT), given their inherent variability and uncertainty in terms of power generation [4–7]. Sharp fluctuations in load demands on a MG constitute additional unpredictable variables [8,9]. However, the impact of these uncertainties can be compensated with the aid of the energy storage system (ESS) [10,11]. Optimal energy scheduling using an ESS is crucial to cope with the uncertainties of RESs and loads, and to ensure the reliable and economical operation of the MG. The MG can operate in the grid-connected and islanded modes [12,13].

MG energy management system (MEMS) successfully provides the reference signals in real time and scheduling time horizons, so that the MG operates in both modes reliably.

Single-stage approaches have been popular because they are easy to implement [14–21]. In reference [14], online optimal control strategies for ESSs was developed. The optimization problem was formulated as a robust mixed integer linear programming (MILP) problem to handle uncertainty in the forecast load demands and RESs power generation. In reference [15], a two-layer optimal dispatch model with ESSs and supercapacitors was formulated. An upper layer minimized the total operational costs, and a lower layer then mitigated load fluctuations and RES forecast errors. It demonstrated that two types of energy storage could be utilized in a hierarchical dispatch model. An execution monitoring and replanning approach for optimal 24-h dispatch considering the uncertainties in weather conditions and load profiles were developed in [16]. A multi-objective function was devised to minimize energy losses, fuel costs, and carbon dioxide emissions. However, the single-stage approaches in [14–16] were modeled only using numerical software.

Some studies have focused on actual-to-laboratory-scale MGs [17–21]. An energy management system (EMS) was proposed to minimize the overall operations costs in [17]. It considered a complete non-linear optimal power flow problem, which determined the active and reactive power injections at all network buses. It compared the solution that derived using a linearized optimal power flow problem. Optimal operation of an isolated system using a virtual power producer was proposed to minimize the generation costs and optimize battery charging/discharging in [18]. Reference [19] proposed the use of offline scheduling to minimize operating costs by using day-ahead forecast data. It focused on modeling a MG and design of an EMS. An EMS maximizing total MG profit considering the total capacities of the RESs and storage systems in terms of future expansion was developed in [20]. Reference [21] proposed the use of an EMS based on unit commitment with a rolling horizon to reduce the uncertainties of forecasting. The goal of their proposed optimization was to minimize the operational costs of the MG.

However, the day-ahead single-stage approach is vulnerable to forecasting errors and unpredictable variations in renewable power generation and load demands. Thus, the optimal operating schedule obtained using a single-stage approach may not guarantee optimal operation of an actual MG. Such issues focus attention on two-stage scheduling approaches, which are robust under forecasting errors and unpredicted changes in operation conditions [22]. Most literature on the two-stage scheduling approach has focused on simulation-level demonstrations [23–29]. Reference [23] addressed energy resources scheduling for the day-ahead and in real time to minimize the total operation cost of a grid-connected MG. It considered the case where all types of loads were imposed in a demand response program. In references [24,25], day-ahead scheduling determined the hourly generation schedules to minimize MG operation costs. Real-time scheduling at a time scale of 5 min allowed the MG to follow the day-ahead scheduled power exchange with the main grid. Two different time scales were applied; 1 h for cooling energy and 5 min for electrical energy. In reference [26], each stage of the two-stage scheduling was two-level. The lower level of the day-ahead scheduling module was to maximize the expected profit, and the upper level was to minimize the total cost of MG operation during the day. The second stage featured hour-ahead scheduling at 15-min intervals. The aim of the lower level of the second stage was to maximize the use of RESs when following the day-ahead schedule. The upper level of the second stage was the same as the upper level of the first stage. A two-stage robust optimization method to plan ESS charging/discharging, and direct load control (DLC) was developed to maximize the total profit of the MG in [27]. In the first stage, ESS charging/discharging power was scheduled to decrease energy purchases from the main grid, and DLC scheduling was then set 15 min earlier to complement ESS operation. In reference [28], hourly scheduling of the day-ahead optimal economic dispatch was performed to minimize the daily MG operational costs, followed by intra-hour adjustment using two layers to smooth fluctuations and follow day-ahead scheduling. In the second stage, two different dispatch time intervals were set, one for virtual energy storage system and the other for the vehicle-to-building system. In reference [29],

a two-stage scheduling framework optimization problem was formulated to optimize the real-time operation of a battery and an ultracapacitor. Hour-ahead scheduling was first performed to minimize the operation cost of the MG, followed by real-time scheduling to eliminate power imbalances caused by the uncertainties in the RESs and loads.

Only a few studies have validated the two-stage optimization problem using real MGs [30,31]. A heuristic optimal operation was proposed to minimize the MG operating cost in [30]. The proposed strategy featured both day-ahead and real time scheduling and performance of three different heuristic algorithms was compared. Reference [31] assessed peak load shifting, onsite PV performance and grid support by formulating an MILP optimal dispatch problem, featuring both month-ahead and day-ahead scheduling. The first stage determines DERs scheduling to minimize total operating costs (on a monthly basis), and the second stage then considers the same optimization problem but over a day-long time horizon. Table 1 presents a summary of previous studies on the optimal scheduling optimization problem types, and the validation methods used.

Table 1. Summary of previous studies on the optimal scheduling using ESS in MG.

Ref.	Problem Types [1]				Validation Methods [2]
	SS	TS	S	I	Test-Bed
[14]	√		√		Grid-connected MG
[15]	√		√		Grid-connected MG
[16]	√		√		Centro Elettrotecnico Sperimentale Italiano, Italy
[17]	√			√	University of Genoa Smart Polygeneration Microgrid, Italy
[18]	√			√	Budapest Tech Renewable Equipment, Hungary
[19]	√			√	MG Research Laboratory in Aalborg University, Denmark
[20]	√			√	Institue of Nuclear Energy Research MG, Taiwan
[21]	√			√	Huatacondo village, Chile
[23]		√	√		Grid-connected MG in distribution network
[24,25]		√	√		Cooling and electricity coordinate MG
[26]		√	√		14 bus radial system
[27]		√	√		IEEE 33 bus radial system
[28]		√	√		MG in an office building
[29]		√	√		7 bus MG
[30]		√		√	Islanded Catalonia Institute for Energy Research MG
[31]		√		√	University of California San Diego, USA

[1] **SS**: Single-Stage, **TS**: Two-Stage. [2] **S**: Simulation level, **I**: Implementation level.

This paper proposes a two-stage scheduling, which consists of the day-ahead scheduling and the hour-ahead scheduling with consideration of the ESS. It is implanted in a MEMS in a campus MG and then validated both in actual case and in simulation to show the effectiveness of the proposed method. The main contributions of this paper are as follows:

- This paper proposes two-stage scheduling—day-ahead and hour-ahead scheduling—to mitigate uncertainty and forecasting errors. The first stage is performed one day in advance to minimize the operation cost, while the second stage is performed every 5 min to minimize the difference between the input power from the main grid before the day and that during the day.
- Unlike previous papers [23–29], we engage in practical implementation of the proposed two-stage scheduling system. An Internet-of-Things (IoT)-based campus MG, composed of PV and ESS, is used as a case study to evaluate the proposed method. The method is developed using not only the forecast data on load demand and required PV generation but also actual data on electricity prices and device parameters.

- The proposed scheduling optimization problem is modelled in PuLP (i.e., a modeling environment in Python) using an open-source solver coin-or branch and cut (CBC). The optimization module in the implemented MEMS is completely open-source based.
- Additional case studies are performed to deal with limitations of the implementation in the campus MG. We verify that completely open-source software can be used to develop the small-scale MG and that the algorithm is applicable at various PV and battery capacities.

The remaining manuscript of this paper outlines as follows: Section 2 describes an overview of the implemented campus MG; Section 3 formulates our proposed two-stage scheduling; Section 4 describes the results of not only implementation but also simulation case studies; and Section 5 concludes the paper. Note that this paper focuses especially on optimization.

2. Overview of the Implemented IoT-Based Campus MG

2.1. Description of the Implemented Campus MG

Figure 1 presents the architecture of the campus MG. The MG ensures uninterrupted operation of critical loads in the library (S-01). As shown in the figure, the MG is grid-connected and includes PV and ESS. The rated PV power of the panels (300 modules) is 100 kW and the panels are installed on the roof of the outdoor parking lot. A total of 250 kWh of lithium-ion batteries (four racks) and a MEMS operating center are situated on the first floor of the library.

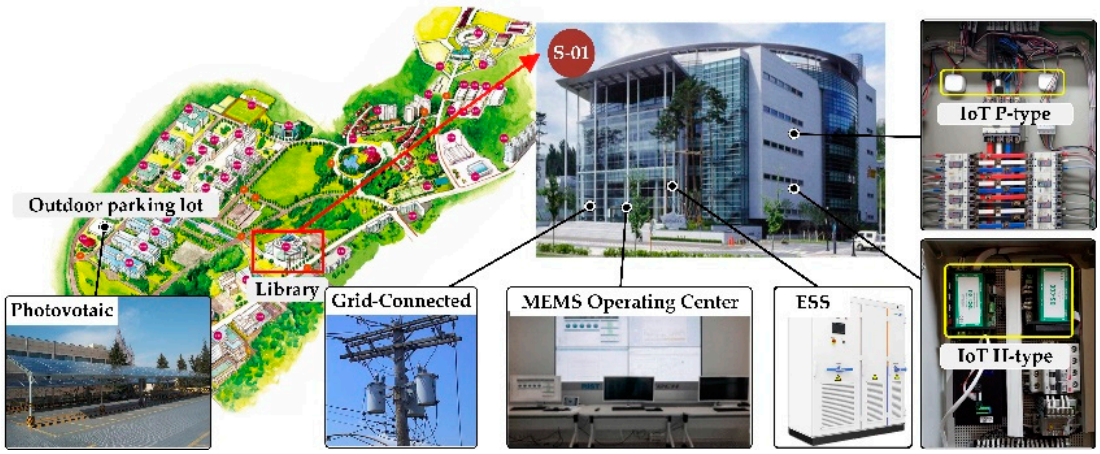

Figure 1. Architecture of the implemented IoT-based campus MG.

Moreover, two types of IoT sensors are installed throughout the library. One is a power sensor (P-type) and the other is a high-speed sensor (H-type). Table 2 lists the features of the two types of sensor. The reliability of sensors is important since inaccurate sensing and data measurement can cause various malfunctions in the EMS and consequently unstable operation of the MG [32]. Note that the average and maximum error rates of two sensors were measured in the field demonstration experiments. 54 P-type sensors have been installed in the electric distribution panels where lighting and plug-in loads are connected. In addition, 23 H-type sensors have been installed in the distribution panels for heating, ventilation, and air conditioning (HVAC) systems (e.g., air cleaners, thermos-hydrostats, package air conditioners, and pumps). The H-type sensors will be more extensively exploited particularly for the analysis of dynamic operation and control of the campus MG, which is considered a next research topic.

Table 2. Features of P-type and H-type IoT sensors.

Types (Number)	Sampling Frequency (Hz)	Average/Maximum Error Rates (%)	Load Types	Information
P (54)	1	0.43/4.94	Lightning and plug-in loads	voltage, current, power factor, active/reactive/apparent power
H (23)	8×10^3	0.50/4.32	HVAC systems	voltage, current, power factor, active/reactive/apparent power frequency, total harmonic distortion/crest factor

2.2. Configuration of an Implemented MG

Figure 2 illustrates the configuration of the campus MG. Existing loads are classified into two types: general loads (e.g., lighting, air conditioners, and heaters) and critical loads (e.g., central computer, super computer, and big-data server). Both types of loads are supplied with power when the MG is in the grid-connected mode. However, in case of failure of the main grid, the general loads may not receive enough power because the critical loads have priority over the general loads.

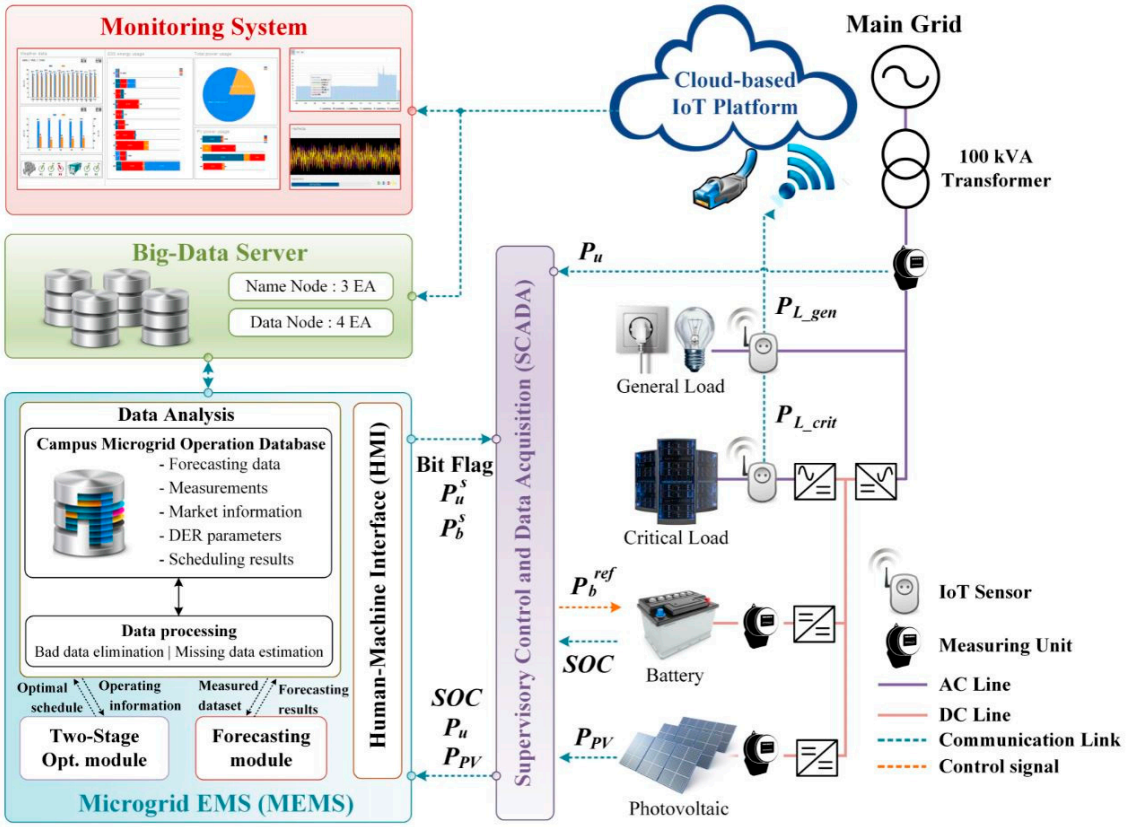

Figure 2. Configuration of the implemented campus MG.

IoT sensors are installed on the sides of the general and critical loads and generate huge amounts of data. All information (e.g., general load power P_{L_gen} and critical load power P_{L_crit} parameters) received by the IoT sensors is transmitted to a cloud-based IoT platform over a communication link [33]. An efficient data communication system is required for continuous, fast, reliable, and accurate transfer of information among sensors. Thus, no disturbance and disconnection is acceptable when sharing information [34]. The P-type sensors use the Ethernet for information transfer, and the H-type sensors communicate via Wi-Fi. The information in the cloud-based IoT platform is sent to a big-data server designed to store and analyze huge amounts of data and to provide a monitoring system. The database (DB) in the MEMS retrieves the required information (e.g., P_{L_gen} and P_{L_crit}) from the big-data server

over the communication link. The MG bus, the PV and the battery are equipped with measuring units. The utility and PV-side units measure voltage, current, active power (i.e., utility power P_u, PV power P_{PV}). An additional state-of-charge (SOC) is measured at the battery side measuring units. All of these data pass through a supervisory control and data acquisition (SCADA) system and are then forwarded to the MEMS; the DB then acquires the data.

The MEMS consists of four modules: forecasting, optimization, data analysis, and human-machine interface (HMI) [35]. The forecasting module operates at different time scales: day-ahead and 2 hours-ahead. It provides forecasts of PV generation power and load demands and delivers the forecasts to the optimization module. The optimization module makes decisions scheduled utility power ${P_u}^s$ and battery power ${P_b}^s$ using data from the forecasting module and DB. Note that the campus MG is implemented using two-stage scheduling, which is described specifically in Section 3. The battery power reference signal ${P_b}^{ref}$ is transferred to the battery controllers through the SCADA, which compensates for any mismatch between the scheduled power and the actual MG power [19]. A bit flag (0/1) is also delivered to the SCADA to decide whether the scheduled results are performed or not in practice. It is zero only when the parameters input by the MEMS operator exceed bounds or when required data (e.g., the forecast load demands and PV generation power, market information, and measurements) are not delivered to the optimization module. The MEMS collects vast amounts of data such as forecasts, measurements, market information, DER parameters, and the result of scheduling. These data must be analyzed properly to provide insights on how to improve the performance of the forecasting and optimization modules [36]. A MEMS should also provide real-time monitoring and control of a MG. This is performed by the HMI, and keeps operators aware of current MG status and delivers accessible information [36]. Turning briefly to communication, no standard form of communication for MEMS operations has yet been defined [37]. However, as the numbers of DERs in MGs increase, a new type of communication system is needed to improve the quality and stability of the system. For example, IEC 61850 deals with real-time supervision and control of electrical systems and is widely used to exchange real-time information [38].

3. The Proposed Two-Stage Scheduling Algorithm

In practice, variations between forecast data and real-time data are inevitable due to variations and uncertainties in load demands and PV generation. However, it is possible to obtain more accurate forecasts as real-time operation becomes more imminent [26,27]. Thus, it is not possible to use only day-ahead scheduling at 1-hour intervals to reflect variability well [29]. Thus, the two-stage scheduling is proposed to mitigate forecast errors and improve the accuracy of scheduling. Figure 3 presents the time framework of our proposed scheduling for the campus MG, which includes day-ahead scheduling and hour-ahead scheduling, especially at a typical time $t = N$ (hour) for Δt where $N \in \{0, 1, \cdots, 23\}$. Also, both stages are formulated as MILP problems, the objective functions of which include penalty terms.

1. Day-ahead scheduling stage: This stage is performed only once before the day to determine the optimal scheduling for the next day. The time window (TW) is 24 h, and the time interval (Δt) is 1 h. The scheduled profiles do not change with Δt.
2. Hour-ahead scheduling stage: This is performed every 5 min during the day for peak saving. Note that hour-ahead scheduling is not conducted at the beginning of every 5-min interval, but rather follows the day-ahead scheduled profile. In other worlds, the second stage runs not 12 times but rather 11 times per Δt. The time window is $TW' - k\Delta t'$ where $k \in \{1, \cdots, 11\}$, and the time interval $\Delta t'$ is 5 min. Only the first interval of each run set serves as a final decision and the rest of the intervals are for reference only.

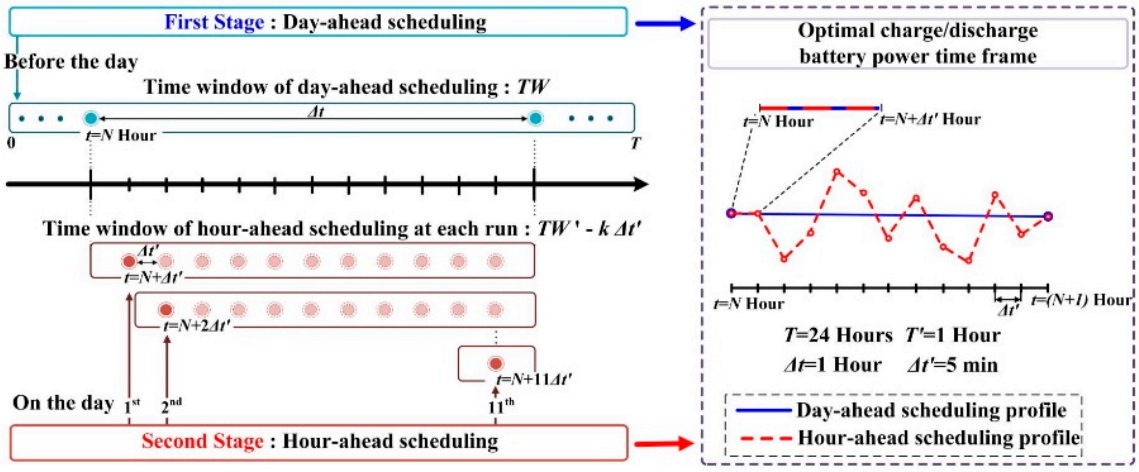

Figure 3. Time framework for the proposed two-stage scheduling.

3.1. Day-Ahead Scheduling Stage

In the first stage, the objective function contains the two terms, shown in Equations (1) and (2). The first term is to minimize the total daily operation cost of the campus MG, and the second is a penalty function that takes into account the situation when the scheduled utility power exceeds the contracted power. Note that it is taken into consideration the case of the MG exporting the surplus PV output power to the main grid, where the scheduled utility power can become negative.

$$\min\{\sum(c_t P_{u,t}^{s,d}) + \theta_1 M_{2,t}\} \forall t \in T, \tag{1}$$

$$M_{2,t} = \max(0, P_{u,t}^{s,d} - P_{cont}) \forall t \in T, \tag{2}$$

where c_t is the hourly electricity price of the main grid. Moreover, ${P_{u,t}}^{s,d}$ is the scheduled utility power imported from the main grid at tth period. Furthermore, P_{cont} is the contracted power and $M_{2,t}$ is an additional decision variable, which is the larger of the 0 and $({P_{u,t}}^{s,d} - P_{cont})$ at time t. In (1), θ_1 is a penalty factor and T is the set of hourly periods (i.e., $T = [0, 1, \cdots, 23]$).

However, the second term needs to be linearized when formulating a MILP problem. It is based on Appendix A and can be achieved using Equations (3)–(5).

$$P_{u,t}^{s,d} = M_{1,t} + M_{2,t} + r_0 \forall t \in T, \tag{3}$$

$$(r_1 - r_0) W_{1,t} \leq M_{1,t} \leq (r_1 - r_0) \tag{4}$$

$$0 \leq M_{2,t} \leq (r_2 - r_1) W_{1,t} \tag{5}$$

where $M_{1,t}$ is a continuous decision variable at time t. Moreover, r_0, r_1, and r_2 are parameters. Furthermore, $W_{1,t}$ is a binary decision variable at time t. All facilitate the piecewise linearization of the penalty function $M_{2,t}$.

Moreover, the power balance between total power production and consumption at any time t must be guaranteed. The linearized DistFlow formulation for the power flow equations is adopted. It has been largely used in both distribution grids and MGs [39,40]. In this paper, we use active power, neglecting power losses on the lines, which can be formulated as Equation (6).

$$P_{u,t}^{s,d} + \sum_{j:(i,j)\in L} P_{j,i,t}^{s,d} = \sum_{k:(k,i)\in L} P_{i,k,t}^{s,d} + \left(P_{ch,t}^{s,d} - P_{dch,t}^{s,d}\right) + \left(P_{L_i,t}^{f,d} - P_{PV,t}^{f,d}\right) \quad \forall i,j,k \in B, \quad \forall t \in T, \tag{6}$$

where ${P_{j,i,t}}^{s,d}$ and ${P_{i,k,t}}^{s,d}$ is the day-ahead scheduled active power that flows from jth bus to ith and from ith bus to kth, respectively, at time t. Moreover, ${P_{Li,t}}^{f,d}$ is the day-ahead forecast load demand

power at ith bus at time t, and ${P_{PV,t}}^{f,d}$ is the forecast PV generation power at time t. In addition, ${P_{ch,t}}^{s,d}$ and ${P_{dch,t}}^{s,d}$ are the day-ahead scheduled battery charge and discharge powers at time t. Furthermore, B is the set of buses and L is the set of lines in the implemented MG. Furthermore, B is the set of buses and L is the set of lines in the implemented MG.

The SOC and power output constraints are important battery issues. Equation (7) shows that the energy stored in the battery at time t is affected by not only its previous value but also the charge and discharge power at the present moment. To prevent the battery from becoming overcharged or overdischarged, the SOC limit must be satisfied, which is described in Equation (8).

$$ {SOC_t}^{s,d} = {SOC_{t-1}}^{s,d} + \left(\left(\eta_{ch} P_{ch,t}^{s,d} - P_{dch,t}^{s,d}/\eta_{dch}\right)\Delta t\right)/EC^{max} \forall t \in T, \tag{7} $$

$$ SOC^{min} \le SOC_t^{s,d} \le SOC^{max} \forall t \in T, \tag{8} $$

where ${SOC_t}^{s,d}$ is the state of charge describing how much energy is stored in the battery at time t. Furthermore, SOC^{min} and SOC^{max} are the minimum and maximum amounts of energy that can be stored in the battery, respectively. Moreover, η_{ch} and η_{dch} are the charge and discharge efficiency of the battery, respectively. In addition, EC^{max} is the capacity of the battery.

Inequality constraints dealing with the charging and discharging power capacity limits of the battery can be derived from Equations (9) and (10). The battery has three operating states: standby, charging, and discharging. The three cannot be in play at the same time t. This can be achieved by introducing a new variable u_t, (i.e., charging/standby (1) and discharging/standby (0)). When the scheduled battery powers ${P_{ch,t}}^{s,d}$ and ${P_{dch,t}}^{s,d}$ are zero, standby is in play.

$$ 0 \le P_{ch,t}^{s,d} \le u_t P_{ch}^{max} \forall t \in T, \tag{9} $$

$$ 0 \le P_{dch,t}^{s,d} \le (1 - u_t) P_{dch}^{max} \forall t \in T, \tag{10} $$

where ${P_{ch}}^{max}$ and ${P_{dch}}^{max}$ are the maximum charge and discharge powers of the battery, respectively. In addition, u_t is a binary variable preventing simultaneous battery charging and discharging.

Another limitation should be satisfied during the operation of the proposed scheduling to meet the scheduling requirements of the next dispatch day and safe operation of the battery [41]. Equation (11) means that the energy stored at the last time of scheduling should be set to its initial value.

$$ SOC_{23}^{s,d} = SOC_{init} \tag{11} $$

where ${SOC_{23}}^{s,d}$ is the scheduled battery SOC at 23:00 p.m.; SOC_{init} is the initial value of the SOC.

3.2. Hour-Ahead Scheduling Stage

The objective function is to minimize the discrepancies between the day-ahead scheduled utility power profiles and the hour-ahead scheduled utility powers, expressed as the first term of Equation (12). Due to natural discharge of the SOC, the actual SOC value could exceed the upper or lower limit. Thus, the second and third terms are added to prevent this situation.

$$ \min\{(|P_{u,t}^{s,d} - P_{u,t}^{s,h}|) - \theta_2 M_{3,t} + \theta_3 M_{5,t}\} \forall t \in T', \tag{12} $$

$$ M_{3,t} = min(0, SOC_t^{s,h} - SOC^{min}) \forall t \in T', \tag{13} $$

$$ M_{5,t} = max(0, SOC_t^{s,h} - SOC^{max}) \forall t \in T', \tag{14} $$

where ${P_{u,t}}^{s,h}$ is the scheduled utility power at time t to be determined in the second stage. Moreover, ${SOC_t}^{s,h}$ represents the scheduled SOC at time t; $M_{3,t}$ is an additional decision variable, which is the smaller of the 0 and $({SOC_t}^{s,h} - SOC^{min})$ at time t. Furthermore, $M_{5,t}$ is another decision variable, which

is the larger of the 0 and $(SOC_t^{s,h} - SOC^{max})$ at time t. In addition, θ_2 and θ_3 are penalty factors and T' is the time set of the second stage (i.e., $T' = [5, 10, \cdots, 1435]$ for the unit time interval of 5 min).

Because the three terms of the objective function are all nonlinear, they must be linearized for the MILP problem. The first term includes an absolute value, which can be changed to a linear form by adding auxiliary variables covering positive and negative deviations. Both the second and third term can be linearized using Equations (15)–(18) in a manner similar to that shown in the first stage, which is also based on Appendix A.

$$SOC_t^{s,h} = M_{3,t} + M_{4,t} + M_{5,t} + r_3 \forall t \in T', \tag{15}$$

$$(r_4 - r_3)W_{2,t} \leq M_{3,t} \leq (r_4 - r_3)\forall t \in T', \tag{16}$$

$$(r_4 - r_3)W_{3,t} \leq M_{4,t} \leq (r_5 - r_4)W_{2,t} \forall t \in T', \tag{17}$$

$$0 \leq M_{5,t} \leq (r_6 - r_5)W_{3,t} \forall t \in T', \tag{18}$$

where $M_{4,t}$ is a continuous variable at time t. Moreover $W_{2,t}$ and $W_{3,t}$ are binary decision variables at time t. In addition, r_3, r_4, r_5 and r_6 are additional parameters. All decision variables are required for piecewise linearization of the penalty functions $M_{3,t}$ and $M_{5,t}$.

The constraints are similar to those imposed on the day-ahead scheduling, except that the SOC limit constraint is considered in the objective function. Note that Equation (23) is appropriate for continuous operations, as is Equation (11), which means that the energy stores of the last frame (running at the final time step) should be equal to the initial values.

$$P_{u,t}^{s,h} + \sum_{j:(i,j)\in L} P_{j,i,t}^{s,h} = \sum_{k:(k,i)\in L} P_{i,k,t}^{s,h} + (P_{ch,t}^{s,h} - P_{dch,t}^{s,h}) + (P_{L_i,t}^{f,h} - P_{PV,t}^{f,h})\forall i, j, k \in B, \forall t \in T', \tag{19}$$

$$SOC_t^{s,h} = SOC_{t-1}^{s,h} + ((\eta_{ch} P_{ch,t}^{s,h} - P_{dch,t}^{s,h}/\eta_{dch})\Delta t)/EC^{max} \forall t \in T', \tag{20}$$

$$0 \leq P_{ch,t}^{s,h} \leq u_t P_{ch}^{max} \forall t \in T', \tag{21}$$

$$0 \leq P_{dch,t}^{s,h} \leq (1 - u_t) P_{dch}^{max} \forall t \in T', \tag{22}$$

$$SOC_{23\_55min}^{s,h} = SOC_{init} \tag{23}$$

where ${P_{j,i,t}}^{s,h}$ and ${P_{i,k,t}}^{s,h}$ is the hour-ahead scheduled active power that flows from jth bus to ith and from ith bus to k_{th}, respectively, at time t. Moreover, ${P_{Li,t}}^{f,h}$ is the hour-ahead forecast load demand power at ith bus at time t, and ${P_{PV,t}}^{f,h}$ is the forecast PV generation power at time t. In addition, ${P_{ch,t}}^{s,h}$ and ${P_{dch,t}}^{s,h}$ are the hour-ahead scheduled battery charge and discharge powers at time t. In (23), ${SOC_{23\_55min}}^{s,h}$ is the scheduled battery SOC at 23:55 p.m.

A surcharging system is considered for the case where the maximum demand power of the 15-min average exceeds the contracted power to stabilize the supply. A constraint in Equation (24) represents this.

$$(P_{u,t-1}^{s,h} + P_{u,t}^{s,h} + P_{u,t+1}^{s,h})/3 \leq P_{cont} \forall t \in T', \tag{24}$$

3.3. Flowchart of the Proposed Two-Stage Scheduling

Figure 4 summarizes the proposed two-stage scheduling for 1 day. This section presents a detailed flowchart.

Step (1) Initialize the time windows TW and TW' as 24 h and 1 h, respectively, and the time intervals Δt and $\Delta t'$ as 1 h and 5 min, respectively. Then, set the current time $t = N + k = 0$.

Step (2) Obtain input information on the ${P_{Li,t}}^{f,d}$, ${P_{PV,t}}^{f,d}$ (time window: TW, time interval: Δt) from the forecast module of MEMS for the first stage, measured SOC data from SCADA, time-of-use (TOU) and ESS parameters from the DB in MEMS.

Step (3) Formulate and solve a MILP optimization problem for the first stage (Section 3.1).

Step (4) Determine $P_{u,t}^{s,d}$, $P_{b,t}^{s,d}$ (time window: TW, time interval: Δt)

Step (5) When time t attains $N+k\Delta t'$, update the input data, which are $P_{Li,t}^{f,h}$, $P_{PV,t}^{f,h}$ (time window: $2TW'$, time interval: $\Delta t'$) from the forecasting module in MEMS for the second stage, measured SOC and utility power from the SCADA, and $P_{u,t}^{s,d}$ from the first-stage.

Step (6) Formulate and solve a MILP optimization problem for the second stage (Section 3.2).

Step (7) Make final decisions on $P_{u,t}^{s,h}$, $P_{b,t}^{s,h}$ (time window: $TW' - (k+1)\Delta t'$, time interval: $\Delta t'$) Note that the time windows of the forecast data and the scheduled profiles differ.

Step (8) If $k \neq 12$ and $N \neq 24$, jump to step 5 after $N = N + 1$, otherwise jump to step 5 after $k = k + 1$.

Step (9) If $N = 24$, obtain the final optimal battery charge/discharge power to minimize MG operation costs.

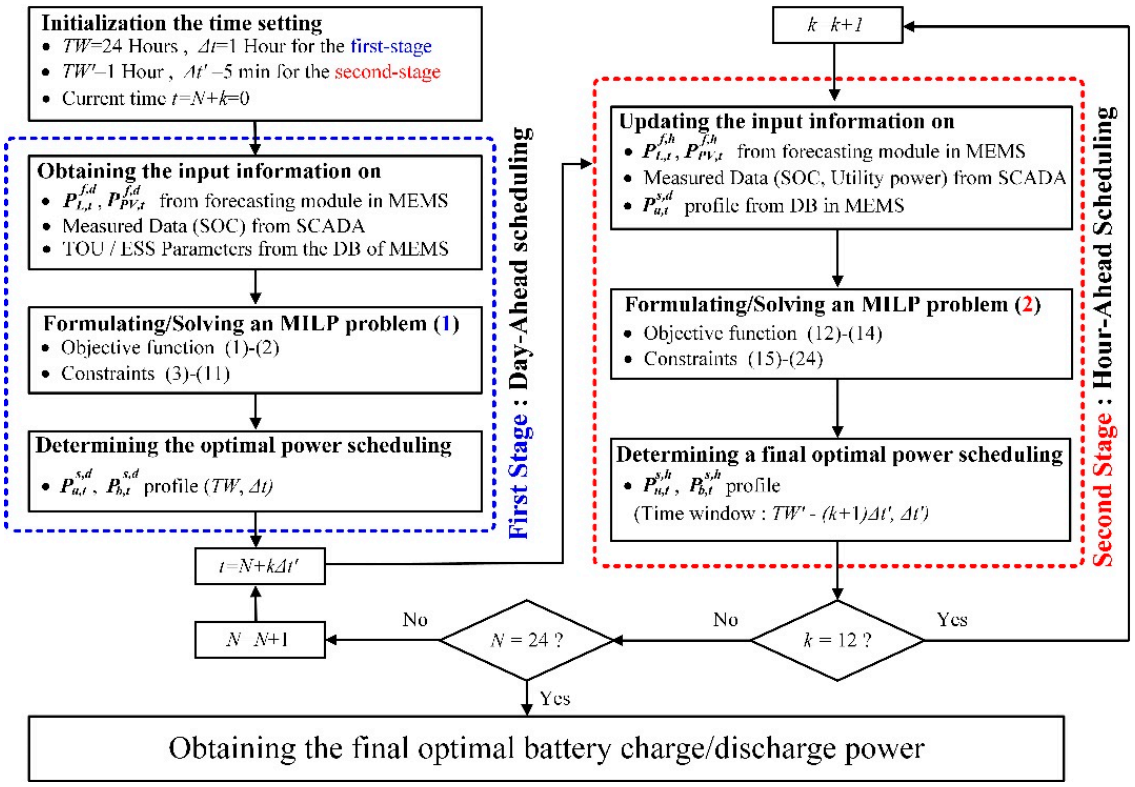

Figure 4. Flowchart of the proposed two-stage scheduling for one day.

4. Case Study and Results

Section 4.1 discusses the implementation results and the effect of hour-ahead scheduling. Section 4.2 discusses other case studies to compare the simulation results obtained not only using different solvers (Section 4.2.1), but also different battery and PV capacities (Section 4.2.2). In the battery scheduling profiles, a negative value indicates the charged state and a positive value means the discharged state. Note that safe battery operation is more important than economical operation in real life, but not during simulation. The run time mentioned Section 4 is the total time that it takes to acquire the input data from the DB, obtain the optimal operating schedules of the ESS, and print out the optimal results to the monitoring system.

4.1. Implementation Results

To evaluate the performance of our proposed two-stage scheduling, we applied it to the campus MG shown in Figure 2 where MEMS ran over the top of Linux. The proposed two-stage scheduling

uses an open-source MILP solver, CBC [42]; an open-source modeling tool PuLP ver. 1.4.6 [43] in the Python environment. Additionally, scheduling was performed using actual data from the forecasting module and the DB in the appropriate time frame.

Table 3 lists the technical parameters of the ESS used. The minimum and maximum SOC values are divided into two types: hard limits SOC_{h_lim} and soft limits SOC_{s_lim}. The values of SOC_{s_lim} are applied to define the SOC limits of the first stage and the SOC penalty functions of the second stage, considering additional reserve in the battery energy capacity. Moreover, the values SOC_{h_lim} are the upper and lower bounds of the second-stage SOC values. The safe, reliable operation of the campus MG is of utmost importance, which could be successfully achieved with the reserve margins of the ESS. SOC have a significant influence on the reserve power of the ESSs [44]. Thus, an additional 5% reserve margin was taken into account in the first stage scheduling, considering that the maximum and minimum SOC levels were set to be 20% and 80%, respectively. In other words, the SOC level could vary between 25% and 75%. The charge and discharge efficiencies of the battery were set to 80%. Table 4 lists the TOU rates for three periods: off-peak (23:00 p.m. ~ 09:00 a.m.), mid-peak (09:00 a.m. ~ 10:00 a.m., 12:00 p.m. ~ 13:00 p.m., 17:00 p.m. ~ 23:00 p.m.), and on-peak (10:00 a.m. ~ 12:00 p.m., 13:00 p.m. ~ 17:00 p.m.). The contracted power was assumed to be 2000 kW. It is also assumed that the selling price for the exported power is assumed to be equal to the buying price for the imported power.

Table 3. ESS parameters.

Parameters	Values	Units
$P_{ch}{}^{max}$	125	(kW)
$P_{dch}{}^{max}$	250	(kW)
EC^{max}	250	(kWh)
$SOC_{h\_lim}{}^{max}$	90	(%)
$SOC_{s\_lim}{}^{max}$	80	(%)
$SOC_{h\_lim}{}^{min}$	10	(%)
$SOC_{s\_lim}{}^{min}$	20	(%)
η_{ch}	80	(%)
η_{dch}	80	(%)

Table 4. Considered TOU price.

Classifications	Time Periods	Prices ($/kWh)
Off-peak	23:00 ~ 09:00	0.0487
Mid-peak	09:00 ~ 10:00 12:00 ~ 13:00 17:00 ~ 23:00	0.0687
On-peak	10:00 ~ 12:00 13:00 ~ 17:00	0.0948

Figure 5 presents HMI screens showing the forecasted and actual loads and the PV generation profiles on the day before and during a typical winter day. The black line represents the day-ahead data for the first stage, the blue line the 2-h-ago data for second stage scheduling, the red line the actual values, and the green histogram the difference between the 2-h-ahead forecast and the actual values. All profiles of Section 4.1 are shown in the HMI at 15-min intervals (kWh). Note that the zero values of the red line at about 17.50 and the blue line at about 19.25 do not indicate faults, rather simply that no data are yet available.

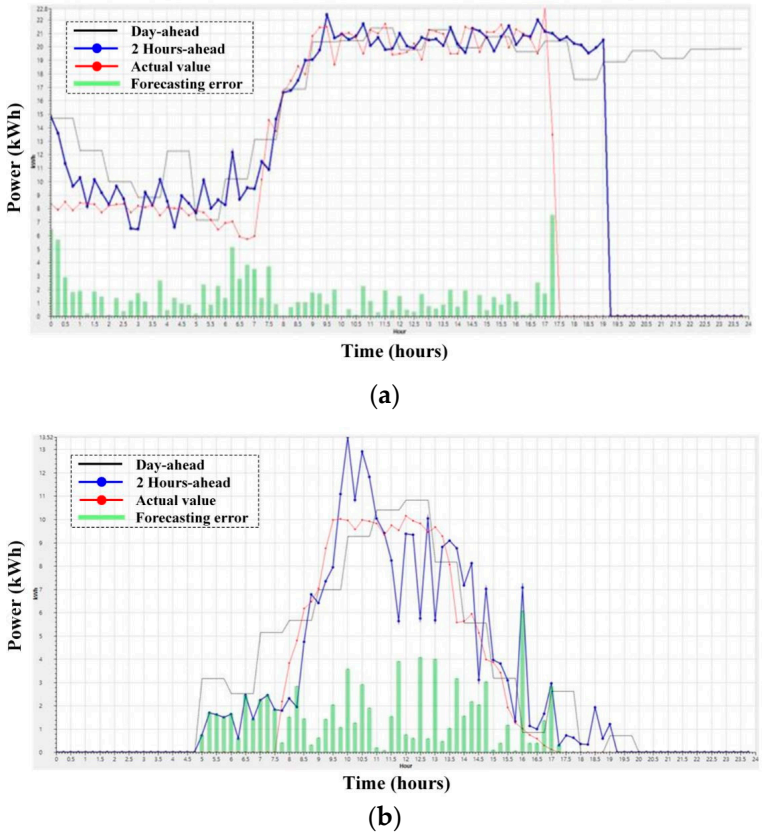

Figure 5. HMI screens of the forecasted and actual profiles before and during a typical winter day (**a**) load; (**b**) PV generation.

4.1.1. Day-Ahead Scheduling

Day-ahead scheduling is performed before the day. The scheduling results in terms of utility power from the main grid and battery charge/discharge powers are shown in Figure 6a, in which the red line indicates the scheduled battery power, the green line the utility power, and the purple line the net load (the difference between the load demand and the PV generation power). The scheduling results of each time step are maintained for 1 h. More utility power is imported when the TOU is low and less when the TOU is high. Also, the ESS is charged when utility power is inexpensive and discharged when it is expensive, to minimize operation costs. The maximum utility power is imported from 08:00 to 09:00 (28.25 kWh per 15 min). The utility power remains within the contracted power because the objective function imposes a large deviation penalty for exceeding the contracted power. However, battery charge/discharge was minimal because the efficiency was assumed to be 80% and a 5% SOC safety margin was applied. The computation time required for a solution was 27.97 s, and the electricity cost was $97.59 during the day.

4.1.2. Hour-Ahead Scheduling

Hour-ahead scheduling makes decision the utility and battery powers every 5 min to minimize deviations between the day-ahead and hour-ahead scheduled utility powers. The results are shown in Figure 6b, in which the colors have the same meanings as in Figure 6a. The total objective value of hour-ahead scheduling is zero, which means that the scheduled utility power of hour-ahead scheduling and that of day-ahead scheduling overlap perfectly. Compared to the day-ahead ESS scheduling, where the ESS is on standby most of the time, the battery is not on standby in the second scheduling stage. The ESS is used to compensate for forecast errors caused by uncertainty and variations in load

demand and PV generation. The battery power changes frequently to ensure that the utility power is equal to that of the day before. The first time interval of hour-ahead scheduling is 6.69 s on average.

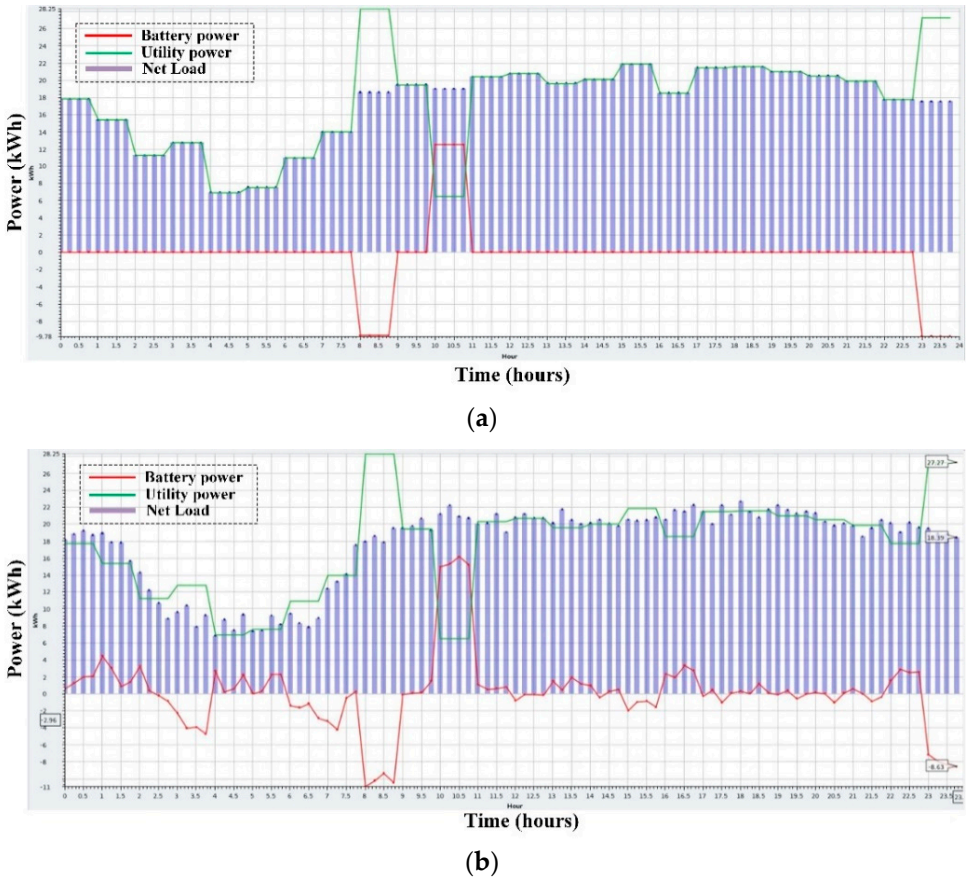

Figure 6. HMI screens showing the scheduled battery power, utility power, and net load of (**a**) day-ahead scheduling; (**b**) hour-ahead scheduling.

4.2. Performance Analysis

In this section, we analyze the performances of open-source solvers and DER capacities at the simulation level. The battery charge and discharge efficiency were both set to 85 %. The other values were unchanged. All simulations were performed using an AMD Ryzen 7 model 1700 eight-core 3-GHz processor with 32.0 GB of memory.

4.2.1. Open-Source Solver Performance

CPLEX is widely used to solve MILP problems. However, the optimization module of our campus MG module is completely open-source. To analyze the performance of the open-source solver, we compared CPLEX and CBC. Both are established in Python. We assumed that the forecast error range between day-ahead and 2-h-ahead would be ±5%, thus relatively small.

Table 5 compares the optimal values and required computation times of two-stage scheduling. The computation times required by the two solvers for day-ahead scheduling were 11.06 s and 0.29 s, respectively. We also compared the average computation times required for the first-time interval of hour-ahead scheduling, because it takes the longest time in the second stage. The times were 3.25s and 0.16 s, respectively. In other words, CBC requires far more computation time than CPLEX for both stages. Figure 7 presents the scheduling imported utility power, battery power, and SOC profiles calculated by the two MILP solvers. This shows that the campus MG worked safely with the reserve margin. The optimal value derived by CBC is exactly that derived by CPLEX for both

day-ahead and hour-ahead scheduling. The simulation results thus show that CBC is acceptable for practical implementation in small-scale MGs even though CPLEX affords better performance in terms of computation time.

Table 5. Comparison results of CBC and CPLEX.

MILP Solvers	Optimal Values ($)		Computation Time (s)	
	Day-Ahead	Hour-Ahead	Day-Ahead	Hour-Ahead [1]
CBC	84.21	0	11.06	3.25
CPLEX	84.21	0	0.29	0.16

[1] First time interval of the hour-ahead scheduling.

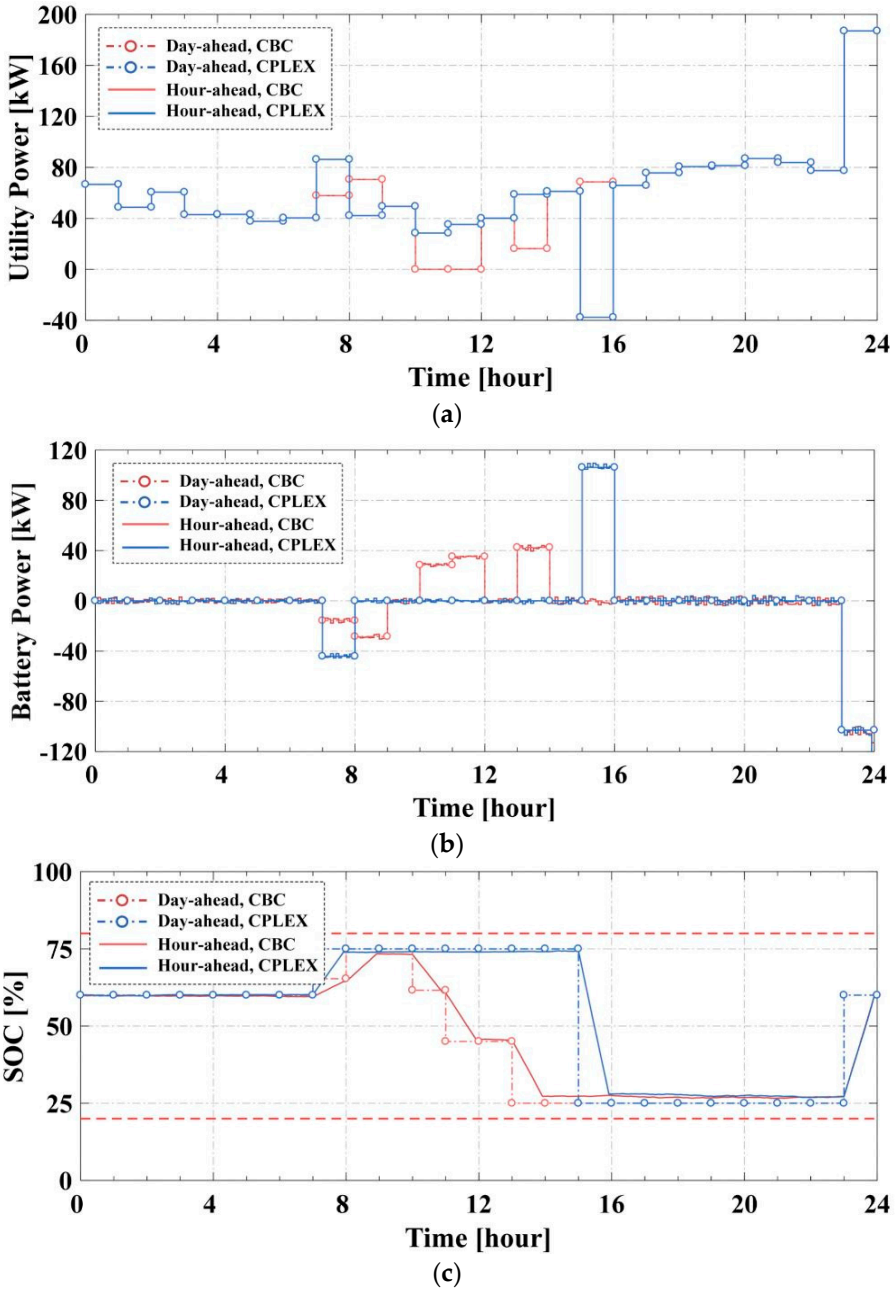

Figure 7. The two-stage scheduling profiles created by the CPLEX and CBC MILP solvers. (**a**) Imported utility power; (**b**) battery power; (**c**) SOC.

4.2.2. DER Capacity Performance

In Section 4.2.2, we compared the operation costs of the first stage as the PV and battery capacities changed. Battery capacity was changed over the range of 100–400 kWh. The PV capacity varied from 0–300 W. Figure 8 presents the MG operating costs within this range. It is assumed that the extent of PV generation at each time is proportional to the PV capacity. The operation costs decreased from about $117.80 to about $49.82 as the PV and battery capacities increased. In other words, the operation costs of the MG are inversely proportional to the PV and battery capacities. However, the PV system affects operating costs more than the battery does. Our findings also demonstrate that our proposed two-stage scheduling algorithm can handle various PV and battery capacities.

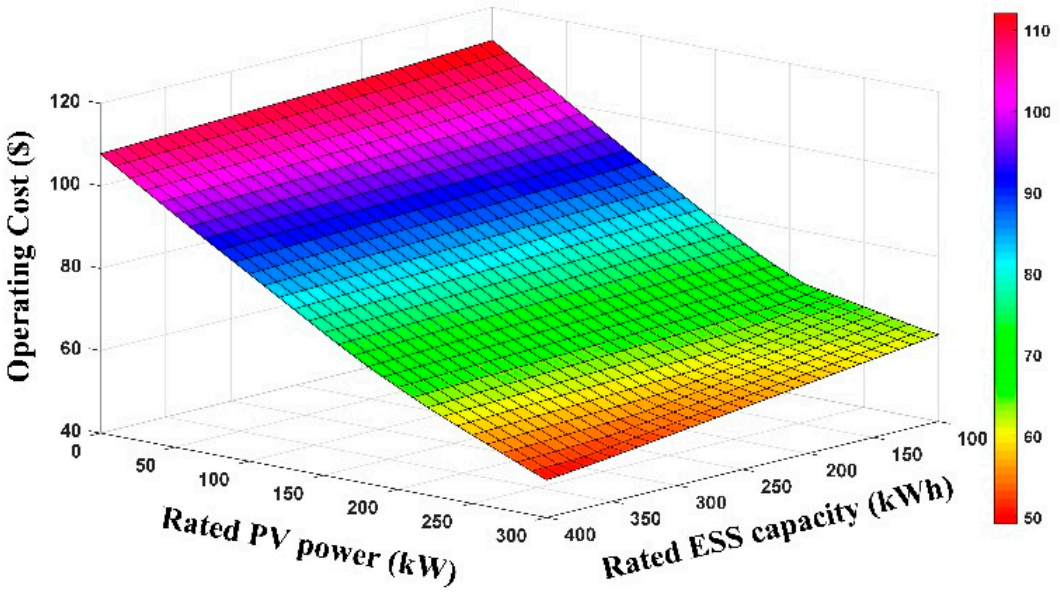

Figure 8. MG operating costs by changes in PV and battery capacities.

5. Conclusions

In this paper, we proposed optimal two-stage scheduling of a MG, considering forecasting errors. It consists of two stages: day-ahead and hour-ahead scheduling. The first stage is performed before the day to minimize operation costs. The second minimizes deviations from the utility powers scheduled by the first stage. The proposed optimal operation system was formulated as an MILP problem and solved by CBC. The application of the proposed method to a real case (a campus MG) proved that our system effectively compensated for forecasting errors and was applicable in practice. Simulations revealed that our proposed scheduling method is also valid during implementations in which the battery is inactivated because of safety concerns. The simulation case studies show that an open-source solver can be used to control small-scale MGs even though the performance is lower than that of a commercial solver; our proposed algorithm is applicable over a wide range of PV and battery capacities.

Further work is required to increase the efficiency of our proposed two-stage scheduling for the campus MG. The error rate of the forecasting module should be decreased, because the economic savings imparted by scheduling improve as the accuracy of forecast data improves. Additionally, our proposed two-stage scheduling algorithm should be implemented using various open- source solvers (e.g., GNU linear programming kit (GLPK), Solving constraint integer programs (SCIP)) or other open-source modeling environments such as Pyomo of Python or JuMP of Julia. We will also measure the required computation times and derive optimal values for larger scale operations in case the campus MG is extended in future.

Author Contributions: Conceptualization, J.-B.I., D.-H.S., and B.-C.J.; methodology, D.-H.S., and B.-C.J.; software, B.-C.J. and D.-H.S.; validation, B.-C.J., D.-H.S., and Y.-J.K.; formal analysis, D.-H.S., and B.-C.J.; investigation, B.-C.J., D.-H.S., and Y.-J.K.; resources, J.-B.I. and B.-C.J.; data curation, D.-H.S., and B.-C.J.; writing—original draft preparation, B.-C.J.; writing—review and editing, B.-C.J., J.-Y.P., D.-H.S., and Y.-J.K.; visualization, B.-C.J. and J.-Y.P.; supervision, Y.-J.K.

Funding: This research was funded by POSCO, grant number 20188018.

Acknowledgments: This work was partly supported by the Korea Institute of Energy Technology Evaluation and Planning (KETEP) grant funded by the Korea government (MOTIE) (No. 70300037). This work was also partly supported by Korea Electric Power Corporation (Grant number: R18XA01).

Conflicts of Interest: The authors declare no conflicts of interest.

Nomenclature

Acronyms

CBC	Coin-or branch and cut
DB	Database
DER	Distributed energy resource
DLC	Direct load control
EMS	Energy management system
ESS	Energy storage system
HMI	Human-machine interface
HVAC	Heating ventilation, and air conditioning
GLPK	GNU linear programming kit
SCIP	Solving constraint integer programs
MEMS	Microgrid energy management system
MG	Microgrid
MILP	Mixed integer linear programming
IoT	Internet-of-things
PV	Photovoltaic
RES	Renewable energy sources
SCADA	Supervisory control and data acquisition
SOC	State-of-charge
TOU	Time-of-use
WT	Wind turbine

Sets and Indices

T	Set of hourly periods in the first stage
T'	Set of 5 min periods in the second stage
B	Set of buses in the MG
L	Set of lines in the MG
i, j, k	Node of electrical network $i, j, k \in B$ and $(i,j), (k,i) \in L$
t	Time periods, $t \in T$ and $t \in T'$ for the first and second stages, respectively
d	Day-ahead stage values
h	Hour-ahead stage values
s	Scheduled values
f	Forecasted values
max, min, ref	Maximum/minimum/reference values
s_lim, h_lim	Soft/hard limit values

Parameters and Constants

TW	Time window for the first stage
TW'	Time window for the second stage
P_{cont}	Contracted power
θ	Penalty factor

Δt	Time interval of the first stage
$\Delta t'$	Time interval of the second stage
r	Parameter for objective function linearization
SOC^{min}, SOC^{max}	Minimum/maximum of the SOC
η_{ch}, η_{dch}	Battery charge/discharge efficiencies
EC^{max}	Battery capacity
${P_{ch}}^{max}$, ${P_{dch}}^{max}$	Maximum charge/discharge power
SOC_{init}	Initial SOC
Variables	
c_t	Hourly TOU price at time t
$P_{u,t}$	Imported power from the utility at time t
M_t	Continuous variable for objective function linearization at time t
W_t	Binary variable for objective function linearization at time t
$P_{i,j,t}$	Power flow from i to j at time t
$P_{L_i,t}$	Load demands at node i at time t
$P_{PV,t}$	PV generation power at time t
$P_{ch,t}$, $P_{dch,t}$	Battery charge/discharge power at time t
SOC_t	SOC at time t
u_t	Binary variable for determining battery charging/discharging at time t

Appendix A

Appendix A.1 Piecewise Linear Approximation of max(0, k_t) Function

Figure A1a shows the piecewise linear approximation of $max(0,k_t)$ function.

Appendix A.1.1 The Objective Function

The objective function is to minimize $max(0,k_t)$, which is described in Equation (A1).

$$\min.max(0, k_t) \tag{A1}$$

where k_t equals to $(x_t - r_1)$.

Appendix A.1.2 Constraints

Equations (A2)–(A5) are required as constraints.

$$M_{2,t} = max(0, k_t)\forall t, \tag{A2}$$

$$x_t = r_0 + M_{1,t} + M_{2,t}\forall t, \tag{A3}$$

$$(r_1 - r_0) \cdot W_{1,t} \leq M_{1,t} \leq (r_1 - r_0)\forall t, \tag{A4}$$

$$0 \leq M_{2,t} \leq (r_1 - r_0) \cdot W_{1,t}\forall t, \tag{A5}$$

where $M_{1,t}$, $M_{2,t}$ and x_t are continuous decision variables at time t. In the day-ahead scheduling stage, x_t is ${P_{u,t}}^{s,d}$. Moreover, r_0, r_1, and r_2 are parameters. Furthermore, $W_{1,t}$ is a binary decision variable at time t. All facilitate the piecewise linearization of the penalty function $max(0, k_t)$. The values of $r_{0–2}$ listed in Table A1. The value of r_0 is determined based on the PV generation power whose rated power is set to 100 kW. Moreover, r_1 is a reference point to determine whether penalty is imposed or not. Furthermore, r_2 represents the limit of the scheduled utility power, which is assumed to be smaller than two times of the contracted power P_{cont}.

Appendix A.2 Piecewise Linear Approximation of {−min(0, s_t) + max(0, l_t)} Function

Figure A1b shows the piecewise linear approximation of $\{-min(0, \underline{s_t}) + max(0, l_t)\}$ function.

Appendix A.2.1 The Objective Function

$$\min.\{-min(0, s_t) + max(0, l_t)\}\forall t, \tag{A6}$$

where s_t and l_t equal to $(x_t - r_4)$ and $(x_t - r_5)$, respectively. Note that s_t is negative.

Appendix A.2.2 Constraints

Equations (A7)–(A12) are required as constraints.

$$M_{3,t} = min(0, s_t)\forall t, \tag{A7}$$

$$M_{5,t} = max(0, l_t)\forall t, \tag{A8}$$

$$x_t = r_3 + M_{3,t} + M_{4,t} + M_{5,t}\forall t, \tag{A9}$$

$$(r_4 - r_3) \cdot W_{2,t} \leq M_{3,t} \leq (r_4 - r_3)\forall t, \tag{A10}$$

$$(r_4 - r_3) \cdot W_{3,t} \leq M_{4,t} \leq (r_5 - r_4) \cdot W_{2,t}\forall t, \tag{A11}$$

$$0 \leq M_{5,t} \leq (r_6 - r_5) \cdot W_{3,t}\forall t \in T', \tag{A12}$$

where $M_{3,t}$, $M_{4,t}$, $M_{5,t}$, x_t are continuous variables at time t. In the hour-ahead scheduling stage, x_t is $SOC_t^{s,h}$. Moreover $W_{2,t}$ and $W_{3,t}$ are binary decision variables at time t. In addition, r_3, r_4, r_5 and r_6 are additional parameters. All decision variables and parameters are required for piecewise linearization of the penalty function $\{-min\ (0, s_t) + max\ (0, l_t)\}$. The values of $r_{3–6}$ listed in Table A1. For the proposed hour-ahead scheduling, r_3 and r_6 are set to the minimum and maximum hard limits on SOC levels, respectively. Moreover, r_4 and r_5 are the minimum and maximum soft limits on SOC values.

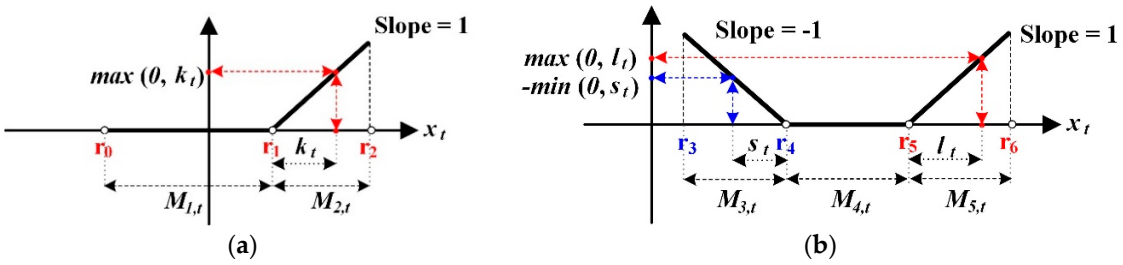

Figure A1. Piecewise linear approximation of penalty functions. (**a**) $max(0, k_t)$ function; (**b**) $\{-min(0, s_t) + max(0, l_t)\}$.

Table A1. Parameter values for the piecewise linearization of the penalty functions.

Day-Ahead Scheduling Stage		Hour-Ahead Scheduling Stage	
Parameters	**Values**	**Parameters**	**Values**
r_0	$-0.5P_{cont}$	r_3	0.1
r_1	P_{cont}	r_4	0.2
r_2	$2P_{cont}$	r_5	0.8
		r_6	0.9

References

1. Hatziargyriou, N.; Asano, H.; Iravani, R.; Marnay, C. Microgrids. *IEEE Power Energy Mag.* **2007**, *5*, 78–94. [CrossRef]
2. Ton, D.T.; Smith, M.A. The U.S. Department of Energy's Microgrid Initiative. *Electr. J.* **2012**, *25*, 84–94. [CrossRef]

3. Katiraei, F.; Iravani, R.; Hatziargyriou, N.; Dimeas, A. Microgrids management. *IEEE Power Energy Mag.* **2008**, *6*, 54–65. [CrossRef]
4. Chen, C.; Duan, S.; Cai, T.; Liu, B.; Hu, G. Smart energy management system for optimal Microgrid economic operation. *IET Renew. Power Gener.* **2011**, *5*, 258–267. [CrossRef]
5. Cong, P.; Tang, W.; Zhang, L.; Zhang, B.; Cai, Y. Day-Ahead Active Power Scheduling in Active Distribution Network Considering Renewable Energy Generation Forecast Errors. *Energies* **2017**, *10*, 1291. [CrossRef]
6. Bakirtzis, E.A.; Biskas, P.N. Multiple Time Resolution Stochastic Scheduling for Systems with High Renewable Penetration. *IEEE Trans. Power Syst.* **2017**, *32*, 1030–1040. [CrossRef]
7. Zhang, Z.-S.; Sun, Y.-Z.; Gao, D.W.; Lin, J.; Cheng, L. A Versatile Probability Distribution Model for Wind Power Forecast Errors and Its Application in Economic Dispatch. *IEEE Trans. Power Syst.* **2013**, *28*, 3114–3125. [CrossRef]
8. Wang, X.; Chen, S.; Zhou, Y.; Wang, J.; Cui, Y. Optimal Dispatch of Microgrid with Combined Heat and Power System Considering Environmental Cost. *Energies* **2018**, *11*, 2493. [CrossRef]
9. Jang, Y.-S.; Kim, M.-K. A Dynamic Economic Dispatch Model for Uncertain Power Demands in an Interconnected Microgrid. *Energies* **2017**, *10*, 300. [CrossRef]
10. Bayod-Rújula, A.A. Future development of the electricity systems with distributed generation. *Energy* **2009**, *34*, 377–383. [CrossRef]
11. Damiano, A.; Gatto, G.; Marongiu, I.; Porru, M.; Serpi, A. Real-Time Control Strategy of Energy Storage Systems for Renewable Energy Sources Exploitation. *IEEE Trans. Sustain. Energy* **2014**, *5*, 567–576. [CrossRef]
12. Cagnano, A.; De Tuglie, E.; Cicognani, L. Prince—Electrical Energy Systems Lab. *Electr. Power Syst. Res.* **2017**, *148*, 10–17. [CrossRef]
13. Moon, H.-J.; Kim, Y.J.; Chang, J.W.; Moon, S.-I. Decentralised Active Power Control Strategy for Real-Time Power Balance in an Isolated Microgrid with an Energy Storage System and Diesel Generators. *Energies* **2019**, *12*, 511. [CrossRef]
14. Malysz, P.; Sirouspour, S.; Emadi, A. An Optimal Energy Storage Control Strategy for Grid-connected Microgrids. *IEEE Trans. Smart Grid* **2014**, *5*, 1785–1796. [CrossRef]
15. Ju, C.; Wang, P.; Goel, L.; Xu, Y. A Two-Layer Energy Management System for Microgrids With Hybrid Energy Storage Considering Degradation Costs. *IEEE Trans. Smart Grid* **2018**, *9*, 6047–6057. [CrossRef]
16. Sanseverino, E.R.; Di Silvestre, M.L.; Ippolito, M.G.; De Paola, A.; Lo Re, G. An execution, monitoring and replanning approach for optimal energy management in Microgrids. *Energy* **2011**, *36*, 3429–3436. [CrossRef]
17. Bracco, S.; Brignone, M.; Delfino, F.; Procopio, R. An Energy Management System for the Savona Campus Smart Polygeneration Microgrid. *IEEE Syst. J.* **2017**, *11*, 1799–1809. [CrossRef]
18. Morais, H.; Kádár, P.; Faria, P.; Vale, Z.A.; Khodr, H.M. Optimal scheduling of a renewable micro-grid in an isolated load area using mixed-integer linear programming. *Renew. Energy* **2010**, *35*, 151–156. [CrossRef]
19. Luna, A.C.; Diaz, N.L.; Graells, M.; Vasquez, J.C.; Guerrero, J.M. Mixed-Integer-Linear-Programming-Based Energy Management System for Hybrid PV-Wind-Battery Microgrids: Modeling, Design, and Experimental Verification. *IEEE Trans. Power Electron.* **2017**, *32*, 2769–2783. [CrossRef]
20. Chen, Y.-H.; Lu, S.-Y.; Chang, Y.-R.; Lee, T.-T.; Hu, M.-C. Economic analysis and optimal energy management models for Microgrid systems: A case study in Taiwan. *Appl. Energy* **2013**, *103*, 145–154. [CrossRef]
21. Palma-Behnke, R.; Benavides, C.; Lanas, F.; Severino, B.; Reyes, L.; Llanos, J.; Saez, D. A Microgrid Energy Management System Based on the Rolling Horizon Strategy. *IEEE Trans. Smart Grid* **2013**, *4*, 996–1006. [CrossRef]
22. Liu, Y.; Nair, N.-K.C. A Two-Stage Stochastic Dynamic Economic Dispatch Model Considering Wind Uncertainty. *IEEE Trans. Sustain. Energy* **2016**, *7*, 819–829. [CrossRef]
23. Zakariazadeh, A.; Jadid, S. Smart Microgrid operational planning considering multiple demand response programs. *J. Renew. Sustain. Energy* **2014**, *6*, 013134. [CrossRef]
24. Bao, Z.; Zhou, Q.; Yang, Z.; Yang, Q.; Xu, L.; Wu, T. A Multi Time-Scale and Multi Energy-Type Coordinated Microgrid Scheduling Solution—Part I: Model and Methodology. *IEEE Trans. Power Syst.* **2015**, *30*, 2257–2266. [CrossRef]
25. Bao, Z.; Zhou, Q.; Yang, Z.; Yang, Q.; Xu, L.; Wu, T. A Multi Time-Scale and Multi Energy-Type Coordinated Microgrid Scheduling Solution—Part II: Optimization Algorithm and Case Studies. *IEEE Trans. Power Syst.* **2015**, *30*, 2267–2277. [CrossRef]

26. Wu, X.; Wang, X.; Qu, C. A Hierarchical Framework for Generation Scheduling of Microgrids. *IEEE Trans. Power Deliv.* **2014**, *29*, 2448–2457. [CrossRef]
27. Zhang, C.; Xu, Y.; Dong, Z.Y.; Ma, J. Robust Operation of Microgrids via Two-Stage Coordinated Energy Storage and Direct Load Control. *IEEE Trans. Power Syst.* **2017**, *32*, 2858–2868. [CrossRef]
28. Jin, X.; Wu, J.; Mu, Y.; Wang, M.; Xu, X.; Jia, H. Hierarchical Microgrid energy management in an office building. *Appl. Energy* **2017**, *208*, 480–494. [CrossRef]
29. Xu, G.; Shang, C.; Fan, S.; Hu, X.; Cheng, H. A Hierarchical Energy Scheduling Framework of Microgrids with Hybrid Energy Storage Systems. *IEEE Access* **2018**, *6*, 2472–2483. [CrossRef]
30. Marzband, M.; Yousefnejad, E.; Sumper, A.; Domínguez-García, J.L. Real time experimental implementation of optimum energy management system in standalone Microgrid by using multi-layer ant colony optimization. *Int. J. Electr. Power Energy Syst.* **2016**, *75*, 265–274. [CrossRef]
31. Sreedharan, P.; Farbes, J.; Cutter, E.; Woo, C.K.; Wang, J. Microgrid and renewable generation integration: University of California, San Diego. *Appl. Energy* **2016**, *169*, 709–720. [CrossRef]
32. Kabalci, Y. A survey on smart metering and smart grid communication. *Renew. Sustain. Energy Rev.* **2016**, *57*, 302–318. [CrossRef]
33. Manur, A.; Venkataramanan, G.; Sehloff, D. Simple electric utility platform: A hardware/software solution for operating emergent Microgrids. *Appl. Energy* **2018**, *210*, 748–763. [CrossRef]
34. Zia, M.F.; Elbouchikhi, E.; Benbouzid, M. Microgrids energy management systems: A critical review on methods, solutions, and prospects. *Appl. Energy* **2018**, *222*, 1033–1055. [CrossRef]
35. Su, W.; Wang, J. Energy Management Systems in Microgrid Operations. *Electr. J.* **2012**, *25*, 45–60. [CrossRef]
36. Lee, E.-K.; Shi, W.; Gadh, R.; Kim, W. Design and Implementation of a Microgrid Energy Management System. *Sustainability* **2016**, *8*, 1143. [CrossRef]
37. Kim, Y.-J.; Wang, J.; Lu, X. A Framework for Load Service Restoration Using Dynamic Change in Boundaries of Advanced Microgrids With Synchronous-Machine DGs. *IEEE Trans. Smart Grid* **2018**, *9*, 3676–3690. [CrossRef]
38. Pinceti, P.; Vanti, M. An Algorithm for the Automatic Detection of Islanded Areas Inside an Active Network. *IEEE Trans. Smart Grid* **2015**, *6*, 3020–3028. [CrossRef]
39. Chen, C.; Wang, J.; Qiu, F.; Zhao, D. Resilient Distribution System by Microgrids Formation After Natural Disasters. *IEEE Trans. Smart Grid* **2016**, *7*, 958–966. [CrossRef]
40. Wang, Z.; Wang, J. Service Restoration Based on AMI and Networked Microgrids Under Extreme Weather Events. *IET Gener. Transm. Distrib.* **2017**, *11*, 401–408. [CrossRef]
41. Nemati, M.; Braun, M.; Tenbohlen, S. Optimization of unit commitment and economic dispatch in Microgrids based on genetic algorithm and mixed integer linear programming. *Appl. Energy* **2018**, *210*, 944–963. [CrossRef]
42. CBC Solver. Available online: https://projects.coin-or.org/Cbc (accessed on 21 March 2019).
43. PuLP. Available online: https://www.coin-or.org/PuLP/ (accessed on 21 March 2019).
44. Cagnano, A.; Caldarulo Bugliari, A.; De Tuglie, E. A cooperative control for the reserve management of isolated Microgrids. *Appl. Energy* **2018**, *218*, 256–265. [CrossRef]